SARS CoV Main Proteinase: The Monomer−Dimer Equilibrium Dissociation Constant

Vito Graziano,[‡] William J. McGrath,[‡] Lin Yang,[§] and Walter F. Mangel*[,‡]

Biology Department, Brookhaven National Laboratory, Upton, New York 11973, and National Synchrotron Light Source, Brookhaven National Laboratory, Upton, New York 11973

Received August 24, 2006; Revised Manuscript Received September 22, 2006

ABSTRACT: The SARS coronavirus main proteinase (SARS CoV main proteinase) is required for the replication of the severe acute respiratory syndrome coronavirus (SARS CoV), the virus that causes SARS. One function of the enzyme is to process viral polyproteins. The active form of the SARS CoV main proteinase is a homodimer. In the literature, estimates of the monomer−dimer equilibrium dissociation constant, K_D, have varied more than 650000-fold, from <1 nM to more than 200 μM. Because of these discrepancies and because compounds that interfere with activation of the enzyme by dimerization may be potential antiviral agents, we investigated the monomer−dimer equilibrium by three different techniques: small-angle X-ray scattering, chemical cross-linking, and enzyme kinetics. Analysis of small-angle X-ray scattering data from a series of measurements at different SARS CoV main proteinase concentrations yielded K_D values of 5.8 ± 0.8 μM (obtained from the entire scattering curve), 6.5 ± 2.2 μM (obtained from the radii of gyration), and 6.8 ± 1.5 μM (obtained from the forward scattering). The K_D from chemical cross-linking was 12.7 ± 1.1 μM, and from enzyme kinetics, it was 5.2 ± 0.4 μM. While each of these three techniques can present different, potential limitations, they all yielded similar K_D values.

Severe acute respiratory syndrome (SARS)[1] was a major, worldwide, public health concern in 2003 (*1*−*3*). More than 8000 cases of this severe, atypical pneumonia were reported, and more than 900 people died (*4*−*7*). A new coronavirus, named SARS coronavirus (SARS CoV), was identified as the causative agent of SARS (*6*, *7*). Coronaviruses are positive-stranded RNA viruses with the largest viral RNA genomes known. The genome of the SARS CoV was sequenced (*8*, *9*). The organization of the genome is similar to that of other coronaviruses. The SARS coronavirus replicase gene gives rise to two overlapping translation products, polyprotein 1a, with a molecular mass of ∼450 kDa, and polyprotein 1ab, with a molecular mass of ∼750 kDa. The replicase protein is conserved among coronaviruses in both length and amino acid sequence. During infection, these two polyproteins are cleaved by virus-coded proteinases, one of which is the 3C-like or SARS CoV main proteinase; proteinase cleavage of the replicase polyproteins releases the individual proteins necessary for virus replication.

The crystal structures of the 3C-like proteinases from transmissible gastroenteritis virus (*10*) and the human coronavirus hCoV 229E (*11*, *12*) have been determined. In the crystal structures, the enzyme is a dimer. The two protomers of the dimer are oriented almost perpendicular to each other. Each protomer contains three domains. Domains I and II have a two-β-barrel fold that is similar to a fold in the chymotrypsin-like serine proteinases. The third domain contains five α-helices; it is connected to domain II by a long loop. Each protomer has its own substrate-binding region situated in the cleft between domains I and II. Domain III is thought to be involved in dimerization (*13*). The SARS CoV main proteinase is a cysteine proteinase with a Cys-His catalytic dyad at the active site (*14*). The SARS CoV main proteinase is conserved among all the SARS coronavirus genome sequences and is highly homologous to other coronavirus 3C-like proteinases.

Since the crystal structures of the 3C-like proteinases in different coronaviruses exhibit similar dimeric structures (*11*, *15*) and since almost all the side chains involved in the formation of the dimer are conserved, it was proposed that the dimer might be the biologically functional form of the 3C-like proteinases (*11*). More recently, Chen et al. (*16*) used molecular dynamic simulations and enzyme activity measurements from a hybrid enzyme to show that only the dimeric form of the proteinase is active.

The equilibrium between the monomer and dimer of the SARS CoV main proteinase has been studied in several laboratories; there is wide disagreement about the monomer−dimer equilibrium dissociation constant, K_D. Fan and coworkers estimated the K_D to be ∼100 μM by analytical gel filtration chromatography (*17*). Consistent with this interpretation was their HPLC-based peptide cleavage assay that

* To whom correspondence should be addressed. Telephone: (631) 344-3373. Fax: (631) 344-3407. E-mail: Mangel@bnl.gov.

[‡] Biology Department.

[§] National Synchrotron Light Source.

[1] Abbreviations: FRET, fluorescence resonance energy transfer; HPLC, high-pressure liquid chromatography; HIV-1, human immunodeficiency virus-1; KSHV, Kaposi's sarcoma-associated herpes virus; SARS, severe acute respiratory syndrome; SAXS, small-angle X-ray scattering; NHS, *N*-hydroxysulfosuccinimide; TCA, trichloroacetic acid; BS^3, bis(sulfosuccinimidyl)suberate; PDB, Protein Data Bank.

10.1021/bi061746y CCC: $33.50
Published on Web 11/17/2006

showed the k_{cat}/K_m varied linearly with the enzyme concentration ranging from 0.9 to 4.5 μM. In an analytical size-exclusion chromatography experiment similar to that by Fan et al. (*17*), but using a lower concentration of enzyme, Chou et al. (*18*) observed one elution peak at 45 kDa. This single elution peak was interpreted as a monomer−dimer mixture and would suggest that the K_D value is much lower. In contrast, enzymatic activity measurements using a more sensitive Dabcyl-Edans FRET pair peptide substrate yielded a K_D of 15 nM (*19*). More recently, Chen and co-workers (*20*) used isothermal titration calorimetry to determine the K_D of full-length and N-terminally deleted SARS CoV main proteinase. Concentrated solutions of SARS CoV main proteinase were sequentially diluted in buffer, and the heat absorbed in the sample cell after each injection was measured. From their analysis of the thermal dilution profile, they estimated a K_D of 227 μM for full-length SARS CoV main proteinase.

Self-association of SARS CoV main proteinase has also been studied extensively by analytical ultracentrifugation (*18*, *21*−*23*). In all of these sedimentation studies, the reported monomer−dimer dissociation constant has varied from 0.35 nM to 14 μM. Because of this almost 650000-fold discrepancy between K_D values, because of the biological importance of the equilibrium in the activation of the enzyme, and because agents that interfere with the dimerization processes may be antiviral agents, we investigated the equilibrium between the monomer and dimer of the SARS CoV main proteinase. We used three different techniques: small-angle X-ray scattering, chemical cross-linking, and enzyme kinetics.

MATERIALS AND METHODS

Materials. Bis(sulfosuccinimidyl)suberate (BS^3) was obtained form Pierce Chemical Co. Bovine serum albumin (BSA) and ovalbumin were obtained from Sigma Chemical Co. The SARS CoV main proteinase and the fluorogenic substrate $(Ala\text{-}Arg\text{-}Leu\text{-}Gln\text{-}NH)_2$-rhodamine were prepared as described previously (*24*). The human adenovirus proteinase (AVP) was purified as described in ref *25*, and human spermidine/spermine acetyltransferase (SSAT) was purified as described in ref *26*.

Small-Angle X-ray Scattering Sample Preparation via Size-Exclusion Chromatography. All samples for small-angle X-ray scattering analysis were chromatographed on a HiLoad 16/60 Superdex 75 column (Amersham Biosciences) to remove any aggregates or high-molecular mass contaminants. Chromatography was performed at room temperature in 25 mM Tris-HCl (pH 7.5) and 150 mM NaCl with a flow rate of 1 mL/min. The peak fractions of each protein were pooled. The concentrations of BSA, ovalbumin, human spermidine/spermine acetyltransferase dimer $[(SSAT)_2]$, and adenovirus proteinase (AVP) were determined spectrophotometrically using molar extinction coefficients at 280 nm of 39 020, 30 230, 35 800, and 26 510 M^{-1} cm^{-1}, respectively. The column was calibrated using molecular mass standards.

Small-Angle X-ray Scattering. Serial dilutions of the SARS CoV main proteinase were created from a stock solution of 13.4 mg/mL (217 μM) to yield samples ranging in concentration from 13.4 to 0.17 mg/mL, in 25 mM Tris-HCl (pH 8), 150 mM NaCl, and 1 mM DTT. The samples were centrifuged at 16000*g* for 30 min prior to being loaded into the capillaries for small-angle X-ray scattering measurements. Solution scattering measurements were performed at station X21A1 at the National Synchrotron Light Source. The X-ray wavelength was 1.089 Å, and the sample−detector distance was 1.71 m. These parameters, together with the beam center position, were calibrated with a silver behenate standard. The sample holder was a 1 mm borosilicate glass capillary (Charles Supper, Natick, MA) that was sealed across the evacuated beam path. Both ends of the capillary were open to allow the sample to flow continuously through the pipet; this minimized X-ray-induced aggregation. Each measurement required ~20 μL of sample and a 15 s exposure time. After each measurement, the capillary was washed repeatedly with buffer solution and purged with compressed nitrogen. The scattering patterns were collected using a CCD detector (Mar USA, Inc., Evanston, IL). The data were averaged into one-dimensional scattering curves using software developed at the beamline; the scattering from the matching buffer solution was subtracted from the data. X-ray transmission data were collected simultaneously with each scattering pattern for use in background subtraction.

Determination of the Dimer−Monomer Equilibrium Dissociation Constant by Fitting the Entire Scattering Curve. Theoretical scattering curves of the dimeric and monomeric forms of the SARS CoV main proteinase were calculated from the dimer crystal structure (*15*) using CRYSOL (*27*). The dimer scattering curve was calculated directly from Protein Data Bank entry 1UK2, while that of the monomer was calculated by removing subunit B from the dimer crystal structure.

The experimental scattering curves of the SARS CoV main proteinase at different concentrations were analyzed using OLIGOMER (*28*). The analysis consisted of fitting the data to a linear combination of the scattering curves of pure monomer and dimer, each weighted by its corresponding volume fraction, which is an adjustable parameter in the regression. The goodness of fit was determined by the χ^2 value, defined as the discrepancy between the calculated and experimental data. The dimer−monomer equilibrium dissociation constant was calculated from a plot of the dimer fraction (f_D) versus the total enzyme concentration in milligrams per milliliter (C_T) by nonlinear regression analysis (single parameter in fit) according to eq 21 and the relation $f_D = 1 - f_M$, where f_M is the monomer fraction.

Estimation of Molecular Masses from the Forward Scatter. The forward scatter [$I(0)$] is the scattered intensity in the direction of the incident beam. It can be determined from a Guinier analysis of the experimental data according to the equation

$$\ln I(q) = \ln I(0) - \frac{q^2 {R_G}^2}{3} \quad (1)$$

where R_G is the radius of gyration and $I(q)$ is the scattered intensity as a function of scattering vector q which is related to the scattering angle (2θ) and the wavelength λ by

$$q = \frac{4\pi \sin\theta}{\lambda} \quad (2)$$

Data in the low-angle region of plots of $I(q)$ versus q^2 can

be fit to a straight line. The forward scatter is obtained from the intercept and R_G from the slope. The forward scatter is related to the molecular mass by (*29*, *30*)

$$I(0) = \kappa N V^2 (\rho - \rho_s)^2 \tag{3}$$

where κ is a constant that includes, among other things, instrument parameters; N is the number of solute molecules per unit volume; V is the volume of the solute; and $\rho - \rho_s$ is the contrast, defined as the difference in the mean electron densities of the solute and solvent. The electron density of the solute is calculated from the chemical composition by the equation

$$\rho = \frac{n_e}{M_r}\frac{N_A}{\bar{\nu}} \tag{4}$$

where N_A is Avogadro's number, n_e is the number of electrons, M_r is the molecular weight, and $\bar{\nu}$ is the partial specific volume of the solute. The electron density of the solvent is assumed to be the same as that of pure water, 0.334×10^{24} e/cm^3. Using the weight concentration (c) instead of number of molecules per unit volume (N), an alternate expression of the forward scatter can be derived by substituting

$$N = \frac{N_A c}{M_r} \tag{5}$$

and since the volume of the solute is

$$V = \frac{\bar{\nu} M_r}{N_A} \tag{6}$$

It follows that

$$I(0) = \kappa M_r c N_A \left(\frac{n_e}{M_r} - \frac{\bar{\nu}\rho_s}{N_A}\right)^2 \tag{7}$$

For molecular weight determinations, a standard curve was constructed by preparing protein standards in the same buffer and measuring their low-angle scattering using the same instrument configuration that was used with the SARS CoV main proteinase samples. A plot of

$$\frac{I(0)/c}{\left(\frac{n_e}{M_r} - \frac{\bar{\nu}\rho_s}{N_A}\right)^2} \tag{8}$$

versus M_r should yield a straight line. The molecular weight of an unknown protein or the weight-average molecular weight from a mixture of proteins can then be determined from the slope and intercept obtained from a linear fit of the data in the standard curve.

Monomer−Dimer Equilibrium and the Forward Scatter Intensity. For a multicomponent system, the experimentally measured forward scatter intensity is a weight-average quantity. The equation that relates the observed forward scatter to the sum of its components will take on slightly different forms depending on the units used to express the concentration: weight per unit volume (e.g., milligrams per milliliter and weight fraction) or number of molecules (e.g., moles, molar concentration, and mole fraction).

For a self-associating system, such as the dimerization reaction of the SARS CoV main proteinase depicted in the scheme below

$$M + M \underset{K_D}{\rightleftharpoons} D$$

the equilibrium dissociation constant, K_D, is defined by

$$K_D = \frac{[M]^2}{[D]} \tag{9}$$

where [M] and [D] are the molar concentrations of the monomer and dimer, respectively.

The total protein concentration ($[M]_T$) expressed in terms of molar monomer equivalents is

$$[M]_T = [M] + 2[D] \tag{10}$$

Since

$$[D] = \frac{[M]_T - [M]}{2} \tag{11}$$

and substituting the above equation into the expression for the K_D yields

$$K_D = \frac{2[M]^2}{[M]_T - [M]} \tag{12}$$

Solving the above quadratic equation for [M] gives

$$[M] = \frac{-K_D + \sqrt{K_D{}^2 + 8[M]_T K_D}}{4} \tag{13}$$

It then follows that

$$[D] = \frac{K_D + 4[M]_T - \sqrt{K_D{}^2 + 8[M]_T K_D}}{8} \tag{14}$$

The measured weight-average forward scatter intensity is given by (*31*)

$$\frac{I(0)}{[M]_T} = \frac{[M] I_M(0)^2 + [D] I_D(0)^2}{[M] I_M(0) + [D] I_D(0)} \tag{15}$$

where $I_M(0)$ and $I_D(0)$ are the forward scatter of the monomer and dimer, respectively.

Alternatively, if the concentration is expressed in terms of weight per unit volume (milligrams per milliliter), then

$$C_T = C_M + C_D \tag{16}$$

where C_M and C_D are the concentrations (milligrams per milliliter) of monomer and dimer, respectively.

Since

$$[M] = \frac{C_M}{M_{rM}} \text{ and } [D] = \frac{C_D}{M_{rD}} = \frac{C_D}{2M_{rM}} \tag{17}$$

where M_{rM} and M_{rD} are the molecular weights of the monomer and dimer, respectively. The expression for the

K_D is

$$K_D = \frac{2C_M^2}{M_{rM}C_D} \quad (18)$$

or

$$K_D = \frac{2f_M^2 C_T}{M_{rM}(1 - f_M)} \quad (19)$$

where f_M and f_D are the weight fractions of monomer and dimer, respectively.

That is

$$f_M = \frac{C_M}{C_T}, f_D = \frac{C_D}{C_T}, \text{ and } f_D + f_M = 1 \quad (20)$$

Solving the quadratic equation for the fraction of monomer, f_M, yields

$$f_M = -K_D M_{rM} + \frac{\sqrt{K_D^2 M_{rM}^2 + 8C_T K_D M_{rM}}}{4C_T} \quad (21)$$

In this case, the measured weight-average forward scatter intensity is given by

$$\frac{I(0)}{C_T} = f_M I_M(0) + f_D I_D(0) \quad (22)$$

Dimer−Monomer Dissociation Constant from the Forward Scatter. The experimentally observed forward scatter $[I(0)/C_T]_{obs}$ from a mixture of proteins is the sum of the individual forward scatter values multiplied by the proportion of each fraction in the mixture. For a monomer−dimer mixture, the observed forward scatter is given by eq 22.

Since $f_D = 1 - f_M$ and the forward scatter, when normalized for concentration, is proportional to the molecular weight, the forward scatter of the dimer is twice that of the monomer, provided that the partial specific volume remains the same upon self-association. Therefore, the equation for calculating the monomer−dimer dissociation constant from a fit of the observed forward scattering intensity normalized to concentration versus total enzyme concentration simplifies to

$$\left[\frac{I(0)}{C_T}\right] = I(0)_M(2 - f_M) \quad (23)$$

where f_M is given by eq 21.

Chemical Cross-Linking of the SARS Main Proteinase. Duplicate samples of the SARS CoV main proteinase were prepared at concentrations of 1, 2.5, 5, 15, and 50 μM with 10 mM HEPES (pH 7.5) and 75 mM NaCl. The volumes of these solutions were 100, 40, 20, 20, and 10 μL, respectively. After equilibration at room temperature for 30 min, a freshly weighed amount of BS^3 was dissolved to a final concentration of 5 mM in 10 mM HEPES (pH 7.5) and 75 mM NaCl and added at a 50-fold molar excess to one of each concentration of the SARS CoV main proteinase solutions. The other samples of the SARS CoV main proteinase received an equivalent volume of buffer alone. The final concentrations of the proteinase in the presence or absence of the BS^3 cross-linker were 0.99, 2.44, 4.76, 13.0, and 25 μM. After incubation for 15 min at room temperature, the 1 and 2.5 μM SARS CoV main proteinase cross-linking and control reactions were stopped by the addition of Tris (pH 7.5) to a concentration of 100 mM. Next, these sets of reactions were incubated for 10 min at room temperature, and the protein was precipitated by addition of deoxycholate to 0.015% and TCA to 7% to concentrate the samples for gel analysis. After centrifugation at 10000*g* for 10 min, the TCA pellets were washed with −20 °C acetone and dissolved in SDS−PAGE sample buffer [62.5 mM Tris (pH 6.8) containing 10% (v/v) glycerol, 2% (w/v) SDS, 2.5% (v/v) mercaptoethanol, and 0.0025% (w/v) bromophenol blue]. The remaining cross-linking and control reactions were stopped by the addition of an equal volume of 2× SDS−PAGE sample buffer [125 mM Tris (pH 6.8) containing 20% (v/v) glycerol, 4% (w/v) SDS, 5% (v/v) mercaptoethanol, and 0.005% (w/v) bromophenol blue]. All the samples were then placed in a boiling water bath for 3 min and subjected to electrophoresis on 14% polyacrylamide gels. The gels were then stained and destained.

A digital image of the gel was acquired using the Bio Doc-It System (UVP). The digital image was processed using Scion Image (Scion Corp) to obtain peak profiles. Peak areas for monomer and dimer bands were calculated using PeakFit (Jandel Scientific). In each lane, a contaminant band, migrating just below the SARS CoV main proteinase band (at approximately 32 kDa), was omitted from the analysis. The amount of monomer remaining for each cross-linking reaction was calculated from the peak areas and compared to non-cross-linked controls. The results were analyzed by nonlinear regression analysis to determine an apparent dimer equilibrium dissociation constant.

Assays of the SARS CoV Main Proteinase. SARS CoV main proteinase in 25 mM Tris-HCl (pH 8) was incubated for 5 min at room temperature or at 37 °C, to allow the monomer−dimer equilibrium to be established. Then, $(Ala\text{-}Arg\text{-}Leu\text{-}Gln\text{-}NH)_2$-rhodamine was added to a final concentration of 20 μM, and the increase with time in absorbance at 496 nm or in fluorescence at 523 nm was measured (*24*). Continuous fluorescence intensity measurements were made with an ISS model PC-1 (ISS, Champaign, IL) photon counting spectrofluorometer. The excitation and emission wavelengths were 492 and 523 nm, respectively, with 8 nm excitation and emission slits. Fluorescence intensity assays were also performed on a TECAN ULTRA 384 plate reader using Greiner black flat bottom 384-well nontreated microplates. The reaction volume was 100 μL. The excitation and emission wavelength filters were set at 485 and 535 nm, respectively. The integration time was 40 μs with 10 lamp flashes per measurement. The time-dependent increase in fluorescence intensity was monitored every 10 s. The instrument gain was set to a value such that the relative fluorescence counts did not saturate the detector during the assay. A standard curve correlating absorbance or fluorescence versus the concentration of the product of the reaction, (Ala-Arg-Leu-Gln-NH)-rhodamine, was used to convert the primary data in an assay, absorbance or fluorescence, to picomoles of substrate hydrolyzed. In all of these assays, the increase in fluorescence with time was linear for at least

5 min during which less than 1% of the substrate was hydrolyzed.

RESULTS

Small-Angle X-ray Scattering: K_D Calculated from the Entire Scattering Curve. A monomer−dimer equilibrium can be characterized by small-angle X-ray scattering. Representative small-angle X-ray scattering curves from solutions of SARS CoV main proteinase at four different concentrations, ranging from 0.7 to 11 mg/mL, are shown in Figure 1A. For comparison, theoretical scattering curves for both the monomer and dimer, calculated as described in Materials and Methods, are also shown in Figure 1A. The solid lines drawn through the experimental data points represent the best fit scattering curves calculated using OLIGOMER (*28*). In all cases, the fits to the experimental data were very good.

The scattering curves from the 11 and 5.5 mg/mL samples of the SARS CoV main proteinase were quite similar to the theoretical scattering curve for the dimer. For example, both scattering curves have a pronounced broad shoulder around $q = 0.17$ Å^{-1} ($d = 36$ Å) that is clearly present in the dimer and becomes progressively less prominent as the enzyme concentration is decreased. It is likely that this secondary maximum represents the spatial correlation between the two monomers in the dimer.

At 1.4 and 0.7 mg/mL, the scattering curves resembled neither that from the dimer nor that from the monomer. This is because the scattering intensity from the dimer is 4 times that of the monomer; hence, the observed scattering intensity, even at the lowest protein concentration, was dominated by the scattering from the dimers. Lower concentrations of the SARS CoV main proteinase could not be used, because the scattering intensity from them could not be detected accurately. For these reasons, a monodisperse solution of monomer could not be characterized.

The monomer and dimer volume fractions, obtained from fitting the entire scattering curves, provided a quantitative interpretation of the small-angle X-ray scattering data. A plot of the dimer volume fraction versus total enzyme concentration is shown in Figure 1B. The data exhibited a hyperbolic-like increase in the dimer fraction, starting from 0.5 at 0.17 mg/mL, the lowest enzyme concentration, and extending to 0.9 at 3 mg/mL. The data from the scattering curves in Figure 1A and data at additional concentrations were used to calculate a dimer−monomer equilibrium dissociation constant, K_D. An equilibrium dissociation constant of 5.8 ± 0.8 μM was calculated by fitting the data in Figure 1B to eqs 20 and 21.

Guinier Analysis of the Scattering Data: Molecular Weight and Radius of Gyration. Guinier analysis of the very low-angle region of the scattering curves in Figure 1 can be used to obtain the molecular weight and radius of gyration, two model-independent parameters that depend on only the size and shape of the macromolecules in solution. For a self-associating system such as this, there is a distribution of macromolecules in which the experimentally measured forward scatter and radius of gyration represent weight-average and *z*-average quantities, respectively. Representative Guinier plots of the SARS CoV main proteinase at two concentrations, 0.17 and 5.5 mg/mL, are shown in Figure 2. For each curve, the small-angle region was fitted using

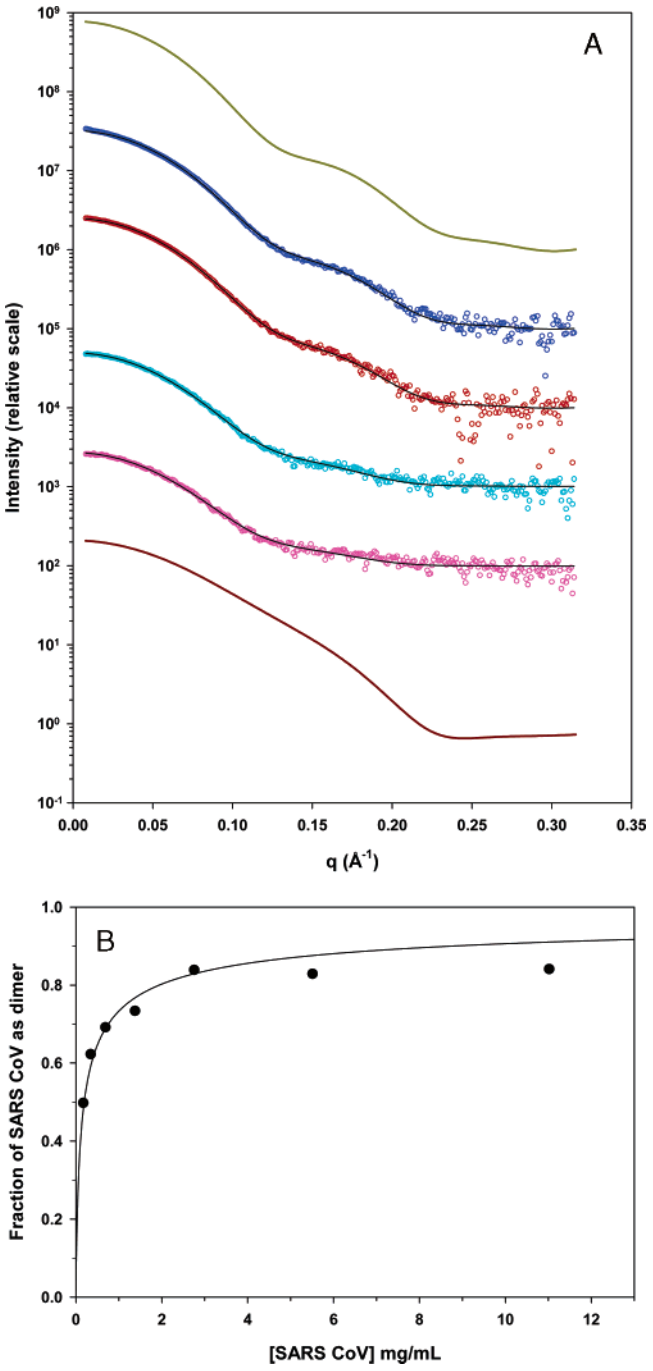

FIGURE 1: Representative small-angle X-ray scattering curves from solutions of the SARS CoV main proteinase (A) and the equilibrium dissociation constant (B). (A) The top curve (dark yellow) is the predicted scattering curve of the dimeric form of the enzyme and the bottom curve (dark red) the predicted scattering curve of the monomer. The scattering curve of the monomer was calculated by stripping one subunit from the dimer crystal structure. Both curves were generated using CRYSOL. The intermediate curves are the experimental scattering data at four different enzyme concentrations: 11 (blue), 5.5 (red), 1.4 (cyan), and 0.7 mg/mL (pink). The curves are displaced vertically relative to each other and are plotted on an arbitrary intensity scale for clarity. For each curve, the experimental data were fit (—) to a linear combination of scattering from the dimer and monomer by OLIGOMER. (B) Volume fractions of dimer obtained from the fits of the data in panel A, plus additional data, were plotted as a function of total SARS CoV main proteinase concentration. The solid line represents the nonlinear regression fit to the data using eqs 20 and 21. The dimer−monomer equilibrium dissociation constant was 5.8 μM.

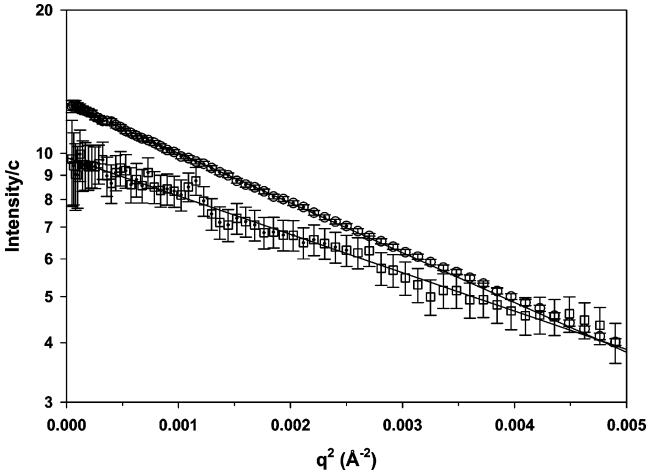

FIGURE 2: Guinier plots derived from low-angle X-ray scattering data of the SARS CoV main proteinase. The protein concentrations were 5.5 (○) and 0.17 mg/mL (□) in 25 mM Tris-HCl (pH 7.5) and 150 mM NaCl. The straight line in each curve is a weighted linear regression fit to the data in the low-angle region within the q^2 range of 0−0.0025 Å^{-2}. The intercept on the ordinate gives the forward scatter, which is proportional to the molecular weight, and the slope is proportional to the square of the radius of gyration. Because of the low protein concentration, the scattering curve for the 0.17 mg/mL solution was considerably noisy when compared to the sample at 5.5 mg/mL.

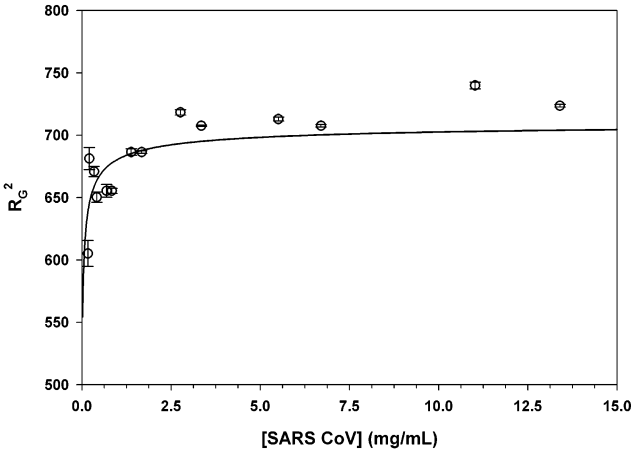

FIGURE 3: Equilibrium dissociation constant obtained from a plot of the square of the radius of gyration as a function of the SARS CoV main proteinase concentration. Small-angle X-ray scattering experiments with different concentrations of the SARS CoV main proteinase were performed to obtain the scattered intensity, $I(q)$, as a function of the scattering vector, q. Guinier analysis of the low-angle part of the data was used to obtain the radius of gyration. Data collected in two different experiments were combined and fit to the monomer−dimer equilibrium model (—) by nonlinear regression to obtain the dissociation constant, as described in the Results. In the fit, the R_G of the monomer was fixed at 22.7 Å and that of the dimer at 26.7 Å.

weighted linear least-squares analysis. The concentration-normalized forward scattering intensity and radius of gyration were calculated from the intercept and slope, respectively. The two lines have significantly different slopes and intercepts. The apparent radii of gyration for the 0.17 and 5.5 mg/mL samples were 24.6 ± 0.21 and 26.7 ± 0.03 Å, respectively. The latter agrees quite well with the R_G of 26.4 Å calculated from the dimer crystal structure, suggesting that at this concentration the enzyme is predominantly in the dimeric form. On the other hand, the measured R_G of 24.6 Å for the 0.17 mg/mL sample is an average value and is consistent with a mixture of monomers and dimers, as shown below.

For a dimer−monomer equilibrium mixture, the mean of the square of the radius of gyration (*29*) is defined by the equation

$$\langle R_G^2 \rangle = \frac{f_M M_M (R_G^2)_M + f_D M_D (R_G^2)_D}{f_M M_M + f_D M_D} \qquad (24)$$

where f_M and f_D are the weight fractions for the monomer and dimer; M_M and M_D are the molecular weights of the monomer and dimer; and $(R_G)_M$ and $(R_G)_D$ are the radii of gyration for the monomer and dimer, respectively.

Since $M_D = 2M_M$ and $f_D = 1 - f_M$, the above expression simplifies to

$$\langle R_G^2 \rangle = \frac{f_M (R_G^2)_M + 2(1 - f_M)(R_G^2)_D}{2 - f_M} \qquad (25)$$

Using the calculated R_G values of 22.7 and 26.7 Å for the monomer and dimer, respectively, and the fractional contribution of each to the scattering (0.5 at 0.17 mg/mL, as shown in Figure 1B), we obtain a value of 25.4 Å for the mean R_G. This is within the experimental error of the empirically determined 24.6 Å R_G. Furthermore, since f_M can be expressed in terms of K_D and total enzyme concentration, the above equation allows one to estimate the dissociation constant from a plot of R_G^2 versus total enzyme concentration. The best fit to the data gave a K_D of 6.5 ± 2.2 (Figure 3).

Small-Angle X-ray Scattering: K_D Calculated from the Forward Scattered Intensity. If there is a dimer−monomer equilibrium, the forward scattered intensity normalized to concentration, which is proportional to the weight-average molecular weight, should increase with an increase in protein concentration. In Figure 4, the concentration-normalized forward scattered intensity is plotted as a function of the total concentration of SARV CoV main proteinase in milligrams per milliliter. The $I(0)/C_T$ increased as the protein concentration was increased, and then it reached a plateau. There was no evidence of a tendency to form higher-order oligomers, even at very high protein concentrations (16 mg/mL). A quantitative analysis of these data incorporated a simple monomer−dimer equilibrium model that related the total protein concentration to the observed forward scattering using the K_D and the forward scatter of a monomeric SARS CoV main proteinase solution, $I(0)_M$, as parameters in the fit. On the basis of eqs 21 and 23, a K_D of 6.8 ± 1.5 μM and an $I(0)_M$ of 6.8 were obtained. The $I(0)/C_T$ values in Figure 4 were then converted to weight-average molecular weights based on the forward scattering intensities of proteins in a protein standard curve. This was done by measuring small-angle X-ray scattering from well-characterized proteins under the same experimental conditions. A plot of the forward scatter normalized for protein concentration and effective number of mole electrons per gram of protein versus the molecular weights of three proteins yielded a linear relationship (Figure 4 inset). The molecular weight standards were the adenovirus proteinase (AVP, 23 087), human spermidine/spermine acetyltransferase dimer [$(SSAT)_2$, 39 786], and ovalbumin (42 750). From this standard curve, the

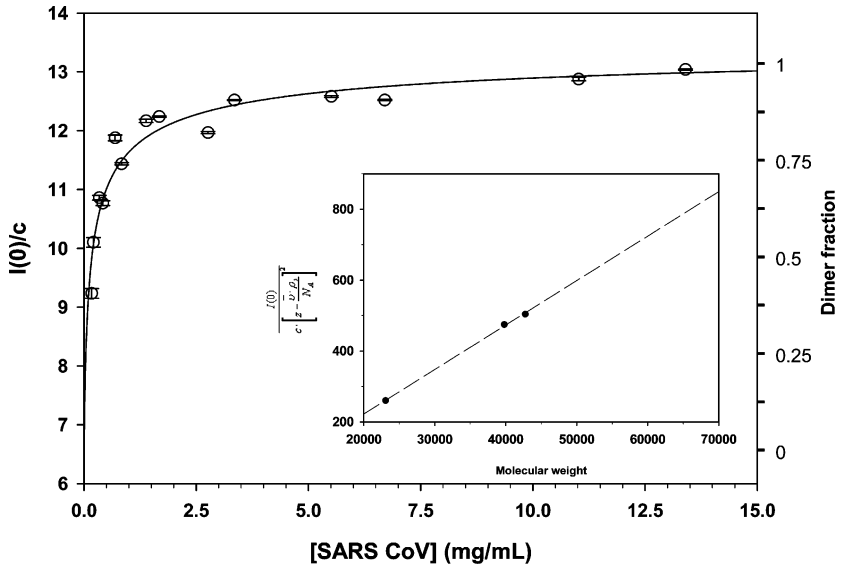

FIGURE 4: Plot of the forward scattered intensity as a function of SARS CoV main proteinase concentration. Small-angle X-ray scattering experiments with different concentrations of SARS CoV main proteinase were performed to obtain the scattered intensity, $I(q)$, as a function of the scattering vector, q. Guinier analysis of the low-angle part of the data was used to obtain the concentration-normalized forward scatter, $I(0)/C_T$, and the radius of gyration. Data collected in two different experiments were combined and fitted to the monomer−dimer equilibrium model by nonlinear regression to obtain the dissociation constant and the forward scatter of monomeric SARS CoV main proteinase, as described in Materials and Methods. The ordinate on the right represents the fraction of dimer present in solution and was calculated by determining the molecular weights of each data point based on the protein standard curve shown in the inset. The standard curve correlates the forward scatter vs protein molecular weight. The forward scatter, normalized for concentration and effective number of mole electrons per gram of protein, is plotted vs the molecular weight of three standard proteins: AVP (M_r = 23 088), SSAT dimer (M_r = 39 786), and ovalbumin (M_r = 42 750). The proteins were in 25 mM Tris-HCl (pH 7.5) and 150 mM NaCl. The dashed line represents the linear regression fit to the data. The parameters obtained from this fit were then used to transform the concentration-normalized forward scatter to molecular weight.

weight-average molecular weight for each data point was calculated and then transformed to dimer fraction, as shown on the right ordinate in Figure 4. The $I(0)_M$ for the monomeric form of SARS CoV main proteinase determined from the nonlinear regression analysis was 6.8. This value agreed very well with the value of 6.6 determined from the protein standard curve for the SARS CoV main proteinase monomer with a molecular weight of 33 759.

Chemical Cross-Linking. Chemical cross-linking with bis(sulfosuccinimidyl)suberate (BS^3) can be used to freeze the dimer in an equilibrium between monomer and dimer. BS^3 is a homobifunctional, water-soluble, noncleavable cross-linker. It contains an amine-reactive *N*-hydroxysulfosuccinimide (NHS) ester at each end of an eight-carbon spacer arm. NHS esters react with primary amines at pH 7−9 to form stable amide bonds, along with release of the *N*-hydroxysulfosuccinimide leaving group. The SARS CoV main proteinase contains six lysine residues at or near the dimer interface (*11*), primary amines that can act as targets for NHS ester cross-linking reagents.

The proteins in the reactions were fractionated by SDS−PAGE, and the gel was stained and destained (Figure 5A). In all lanes, the monomer is present at an approximate molecular mass of 33 kDa. Beginning at lane 7 and continuing through lane 11, the amount of dimer, with an approximate molecular mass of 66 kDa, increased as the total protein concentration was increased. The lanes of the gel were scanned and the areas under the peaks quantified, and the fraction of monomer remaining in each reaction mixture was calculated. A graph of the fraction of dimer yielded a rectangular hyperbola (Figure 5B). From the graph, a dimer−monomer equilibrium dissociation constant (K_D) of 12.7 ± 1.1 μM was calculated.

Kinetic Studies. Kinetic studies indicated that the active form of the SARS CoV main proteinase may be a homodimer. This is true because the initial rate of substrate hydrolysis did not vary linearly with the concentration of the SARS CoV main proteinase, as shown in Figure 6A.

This nonlinearity was most apparent at very low enzyme concentrations where there was little change in the initial rate. However, as the enzyme concentration was increased into the micromolar range, there were large increases in the initial rates with increases in enzyme concentration. Data could not be obtained at enzyme concentrations above 3 μM, because the initial rates of substrate hydrolysis were too fast to be measured in a conventional spectrofluorometer.

The lack of linearity in Figure 6A could be explained by assuming a monomer−dimer equilibrium in which only the homodimer is the active form of the enzyme; i.e., the rate of substrate hydrolysis is proportional to the molar concentration of the dimer in the reaction mixture. The monomer−dimer equilibrium was analyzed according to the scheme

$$M + M \underset{K_D}{\rightleftharpoons} D + S \underset{K_M}{\rightleftharpoons} DS \xrightarrow{k_{cat}} D + P$$

where M and D denote the monomeric and dimeric forms of the enzyme, respectively, DS is the dimer−substrate complex, K_M is the Michaelis constant, k_{cat} is the catalytic rate constant, and P is the product.

The initial rate of substrate hydrolysis, v, is

$$v = k_{cat}[DS] = \frac{k_{cat}}{K_m}[S][D] = A_s[D] \qquad (26)$$

where A_s is the specific activity of the dimer and [D] can be

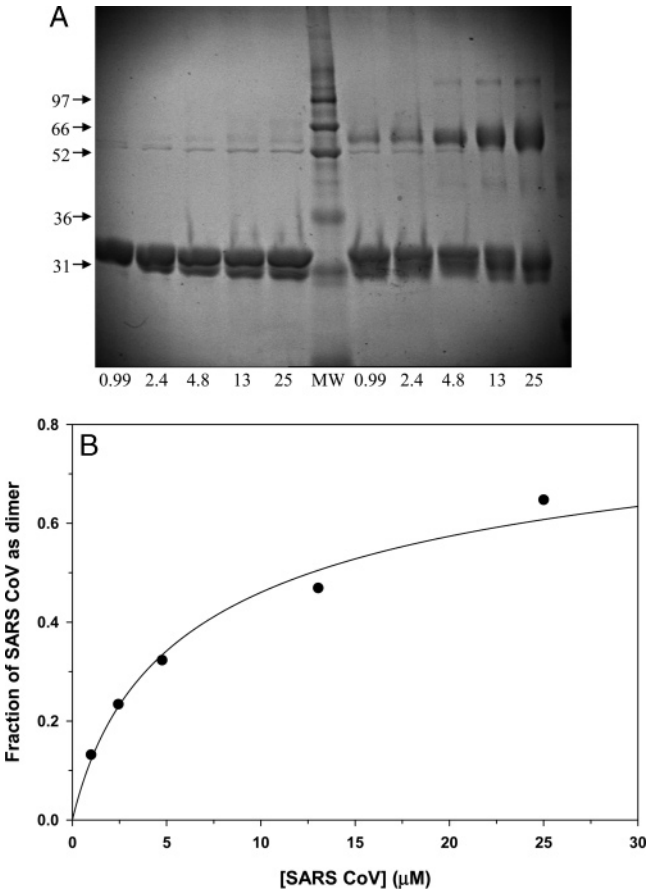

FIGURE 5: Determination of the K_D of the monomer−dimer equilibrium by chemical cross-linking. (A) A SDS−polyacrylamide gel of chemical cross-linking reactions at different concentrations of the SARS CoV main proteinase and (B) a quantitative analysis of the cross-linking reactions. (A) Different concentrations of the SARS CoV main proteinase [1.0 μM (lanes 1 and 7), 2.5 μM (lanes 2 and 8), 5 μM (lanes 3 and 9), 15 μM (lanes 4 and 10), and 50 μM (lanes 5 and 11)] were incubated for 30 min. Then, the chemical cross-linker BS[3] was added to a 50-fold molar excess to the reaction mixtures in lanes 7−11. After 15 min, the proteins in the reactions were fractionated by SDS−PAGE. Molecular weight markers are in lane 6 with their molecular weights at the left edge of the gel. (B) The lanes in the gel in panel A were scanned and the areas under the peaks quantified. The monomer fraction was calculated for each cross-linking reaction. The data are presented as dimer fraction vs the SARS CoV main proteinase concentration in micromolar. The line through the data points was obtained by nonlinear regression analysis using eq 14 and the relation $f_D = 2[D]/[M]_T$. The resultant K_D was 12.7 ± 1.1 μM.

defined in terms of the monomer−dimer equilibrium dissociation constant (K_D) and the total enzyme concentration ($|M|_T$) by eq 14.

A nonlinear regression fit yielded a dissociation constant of 5.2 μM (Table 1) and a specific activity of the dimer (A_s) of 4.1 nM^{-1} s^{-1} μM. The k_{cat}/K_m was 0.21 nM^{-1} s^{-1}.

Now, the hypothesis that the active form of the SARS CoV main proteinase may be a homodimer can be tested by transforming the data in Figure 6A. Using eq 14, the molar concentration of the SARS CoV main proteinase dimer was calculated and the data were replotted as the initial rates versus the dimer concentration (Figure 6B). Instead of a nonlinear variation in the rate, a linear trend in the rate was observed. The data can be characterized as conforming to a straight line going through the origin.

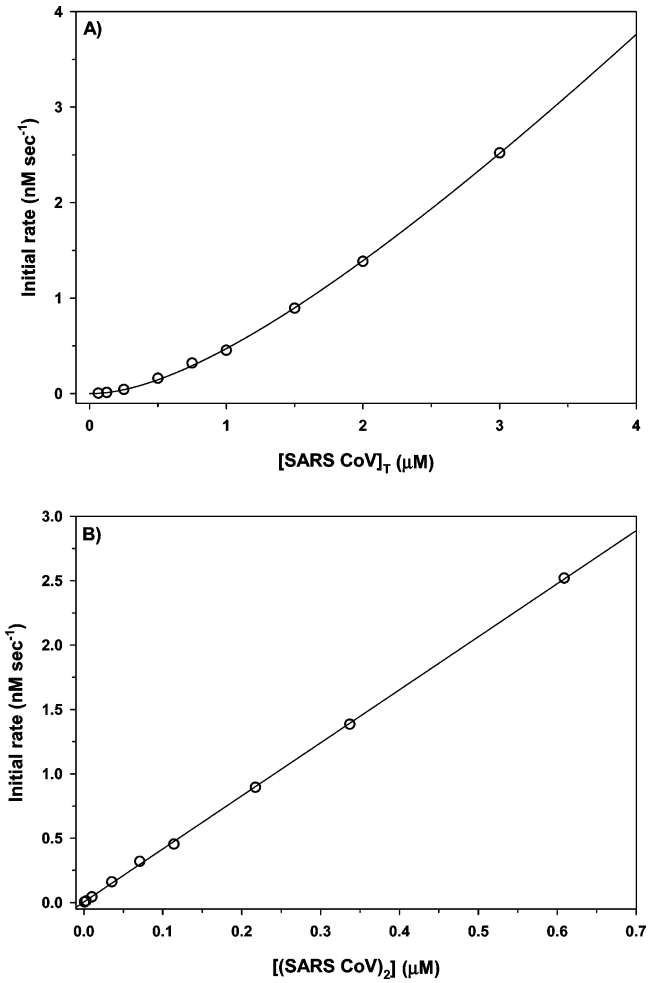

FIGURE 6: Determination of the K_D of the monomer−dimer equilibrium by enzyme kinetics. (A) Rates of substrate hydrolysis by the SARS CoV main proteinase as a function of total enzyme concentration expressed in monomer equivalents and (B) rates of substrate hydrolysis as a function of dimer concentration. SARS CoV main proteinase activity was measured with the fluorogenic substrate (Ala-Arg-Leu-Gln-$NH)_2$-rhodamine. (A) The solid line represents a nonlinear regression fit to the experimental data assuming that only the dimeric form of the enzyme contributes to the observed rate of substrate hydrolysis. By using eq 14, an equilibrium dissociation constant of 5.2 μM was obtained. (B) The dimer concentration was calculated using the K_D determined from the data in panel A.

Table 1: Monomer−Dimer Equilibrium Dissociation Constants of the SARS CoV Main Proteinase Measured by Different Techniques

	K_D (μM)
small-angle X-ray scattering	
entire scattering curve	5.8 ± 0.8
R_G^2	6.5 ± 2.2
forward scattering curve	6.8 ± 1.5
chemical cross-linking	12.7 ± 1.1
enzyme kinetics	5.2 ± 0.4

DISCUSSION

In this study, small-angle X-ray scattering, chemical cross-linking, and enzyme kinetics were used to characterize the oligomeric state of the SARS CoV main proteinase. Both the biochemical and biophysical data were consistent with a monomer−dimer equilibrium that had a dissociation constant of ~6 μM. The small-angle X-ray scattering data clearly showed that the SARS CoV main proteinase is predominantly

dimeric at concentrations above 2 mg/mL. Below 2 mg/mL, the dimer started to dissociate and began to exist in an equilibrium with the monomeric form. Analysis of scattering data from a series of measurements at different SARS CoV main proteinase concentrations yielded K_D values of 5.8 ± 0.8, 6.5 ± 2.2, and 6.8 ± 1.5 μM (Table 1). The K_D from chemical cross-linking was 12.7 ± 1.1 μM, and it was 5.2 ± 0.4 μM from enzyme kinetics.

Each technique used to measure K_D values can present different, specific, problems such that the K_D value that is obtained may not be correct. K_D values obtained by sedimentation equilibrium can be sensitive to pressure. High pressure in the cuvette forces proteins to decrease their volume, leading to unfolding or dissociation of multimeric structures (*32*). The substrate used in enzymatic activity assays may stabilize the dimeric form. Chemical cross-linking with a bifunctional cross-linking reagent requires that the two acceptor side chains in each monomer be near each other in the dimer and that cross-linking not shift the monomer−dimer equilibrium. Some techniques require relatively high concentrations of protein, e.g., small-angle X-ray scattering. Because of this, obtaining data from pure SARS CoV main proteinase monomer was not possible.

The reason three different techniques were used to measure the K_D was to avoid the possibility that some unpredictable characteristic of the dimerization reaction, e.g., pressure sensitivity, might give a misleading results. However, these three different techniques yielded similar results. Thus, variables such the inability to obtain the scattering intensity of the SARS CoV main proteinase monomer, substrate stabilization of the dimer, and the proximity of acceptor side chains in the chemical cross-linking of the dimer did not significantly alter measurement of the K_D.

In the kinetic studies, the equations for activation by dimerization assumed a single product, i.e., one functioning active site in a dimer. Chen et al. (*16*) investigated whether the two protomers in the dimer are active by using molecular dynamics simulations and mutational studies. The molecular dynamics simulations show that the monomers are always inactive, the two protomers in the dimer are asymmetric, and only one protomer is active at a time. A similar conclusion was reached upon mixing wild-type monomers and monomers containing the C145A mutation. Only one active promoter in the dimer is enough for catalysis.

Large discrepancies in K_D values in the literature are not unique to the SARS CoV main proteinase. Equally large discrepancies for the HIV-1 proteinase appear in the literature. Sedimentation studies yield K_D values from <10 nM (*33*) to 52.7 μM (*34*). Kinetic assays yield K_D values for the HIV-1 proteinase from <1 nM (*35*) to 440 nM (*36*). However, these differences, more than 50000-fold, are not as large as the almost 650000-fold difference in K_D values reported for the SARS CoV main proteinase.

Other viruses contain proteinases that become active only upon dimerization. Human cytomegalovirus, a member of the herpes virus family, encodes a serine proteinase that is active only as a dimer. Its K_D is 8 μM (*37*). Another member of that family, Kaposi's sarcoma-associated herpes virus (KSHV), has a proteinase in which significant conformational changes occur upon activation of the monomer by dimerization (*38*). Hepatitis A virus, a picornavirus, encodes a cysteine proteinase with a chymotrypsin-like fold. It forms homodimers with a K_D in the millimolar range; in the presence of viral RNA, the K_D decreases to 8.8 μM (*39*). The dimeric forms of all the above enzymes contain two active sites that are accessible to solvent. In the case of the KSHV proteinase, both sites can be simultaneously active with a small substrate (*38*). In contrast, retrovirus proteinases, e.g., the HIV proteinase, dimerize in a process that creates a single, shared active site at the dimer interface (*40*, *41*).

There are many reasons why the monomers of virus-encoded proteinases are inactive and must form dimers to become active. Dimerization restricts the presence of enzyme activity, in space, to specific sites within the cell and, in time, to a certain time after infection. For example, when initially synthesized, the monomer does not dimerize because its concentration is below the K_D. This prevents cleavage of certain cellular proteins needed by the virus early in infection; it also prevents the premature processing of viral polyproteins. Introduction of a tethered proteinase dimer into a retroviral provirus leads to the loss of infectivity and particle formation, clearly due to the premature activation of the polyprotein processing (*42*, *43*). Allosteric activation seems to be a common mechanism exhibited by a wide variety of proteinases.

REFERENCES

1. Chan, H. L., Tsui, S. K., and Sung, J. J. (2003) Coronavirus in severe acute respiratory syndrome (SARS), *Trends Mol. Med. 9*, 323−5.
2. Leng, Q., and Bentwich, Z. (2003) A novel coronavirus and SARS, *N. Engl. J. Med. 349*, 709.
3. Kuiken, T., Fouchier, R. A., Schutten, M., Rimmelzwaan, G. F., van Amerongen, G., van Riel, D., Laman, J. D., de Jong, T., van Doornum, G., Lim, W., Ling, A. E., Chan, P. K., Tam, J. S., Zambon, M. C., Gopal, R., Drosten, C., van der Werf, S., Escriou, N., Manuguerra, J. C., Stohr, K., Peiris, J. S., and Osterhaus, A. D. (2003) Newly discovered coronavirus as the primary cause of severe acute respiratory syndrome, *Lancet 362*, 263−70.
4. Drosten, C., Gunther, S., Preiser, W., van der Werf, S., Brodt, H. R., Becker, S., Rabenau, H., Panning, M., Kolesnikova, L., Fouchier, R. A., Berger, A., Burguiere, A. M., Cinatl, J., Eickmann, M., Escriou, N., Grywna, K., Kramme, S., Manuguerra, J. C., Muller, S., Rickerts, V., Sturmer, M., Vieth, S., Klenk, H. D., Osterhaus, A. D., Schmitz, H., and Doerr, H. W. (2003) Identification of a novel coronavirus in patients with severe acute respiratory syndrome, *N. Engl. J. Med. 348*, 1967−76.
5. Ksiazek, T. G., Erdman, D., Goldsmith, C. S., Zaki, S. R., Peret, T., Emery, S., Tong, S., Urbani, C., Comer, J. A., Lim, W., Rollin, P. E., Dowell, S. F., Ling, A. E., Humphrey, C. D., Shieh, W. J., Guarner, J., Paddock, C. D., Rota, P., Fields, B., DeRisi, J., Yang, J. Y., Cox, N., Hughes, J. M., LeDuc, J. W., Bellini, W. J., and Anderson, L. J. (2003) A novel coronavirus associated with severe acute respiratory syndrome, *N. Engl. J. Med. 348*, 1953−66.
6. Fouchier, R. A., Kuiken, T., Schutten, M., van Amerongen, G., van Doornum, G. J., van den Hoogen, B. G., Peiris, M., Lim, W., Stohr, K., and Osterhaus, A. D. (2003) Aetiology: Koch's postulates fulfilled for SARS virus, *Nature 423*, 240.
7. Peiris, J. S., Chu, C. M., Cheng, V. C., Chan, K. S., Hung, I. F., Poon, L. L., Law, K. I., Tang, B. S., Hon, T. Y., Chan, C. S., Chan, K. H., Ng, J. S., Zheng, B. J., Ng, W. L., Lai, R. W., Guan, Y., and Yuen, K. Y. (2003) Clinical progression and viral load in a community outbreak of coronavirus-associated SARS pneumonia: A prospective study, *Lancet 361*, 1767−72.
8. Rota, P. A., Oberste, M. S., Monroe, S. S., Nix, W. A., Campagnoli, R., Icenogle, J. P., Penaranda, S., Bankamp, B., Maher, K., Chen, M. H., Tong, S., Tamin, A., Lowe, L., Frace, M., DeRisi, J. L., Chen, Q., Wang, D., Erdman, D. D., Peret, T. C., Burns, C., Ksiazek, T. G., Rollin, P. E., Sanchez, A., Liffick, S., Holloway, B., Limor, J., McCaustland, K., Olsen-Rasmussen, M., Fouchier, R., Gunther, S., Osterhaus, A. D., Drosten, C., Pallansch, M. A., Anderson, L. J., and Bellini, W. J. (2003)

Characterization of a novel coronavirus associated with severe acute respiratory syndrome, *Science 300*, 1394−9.

9. Marra, M. A., Jones, S. J., Astell, C. R., Holt, R. A., Brooks-Wilson, A., Butterfield, Y. S., Khattra, J., Asano, J. K., Barber, S. A., Chan, S. Y., Cloutier, A., Coughlin, S. M., Freeman, D., Girn, N., Griffith, O. L., Leach, S. R., Mayo, M., McDonald, H., Montgomery, S. B., Pandoh, P. K., Petrescu, A. S., Robertson, A. G., Schein, J. E., Siddiqui, A., Smailus, D. E., Stott, J. M., Yang, G. S., Plummer, F., Andonov, A., Artsob, H., Bastien, N., Bernard, K., Booth, T. F., Bowness, D., Czub, M., Drebot, M., Fernando, L., Flick, R., Garbutt, M., Gray, M., Grolla, A., Jones, S., Feldmann, H., Meyers, A., Kabani, A., Li, Y., Normand, S., Stroher, U., Tipples, G. A., Tyler, S., Vogrig, R., Ward, D., Watson, B., Brunham, R. C., Krajden, M., Petric, M., Skowronski, D. M., Upton, C., and Roper, R. L. (2003) The Genome sequence of the SARS-associated coronavirus, *Science 300*, 1399−404.
10. Anand, K., Palm, G. J., Mesters, J. R., Siddell, S. G., Ziebuhr, J., and Hilgenfeld, R. (2002) Structure of coronavirus main proteinase reveals combination of a chymotrypsin fold with an extra α-helical domain, *EMBO J. 21*, 3213−24.
11. Anand, K., Ziebuhr, J., Wadhwani, P., Mesters, J. R., and Hilgenfeld, R. (2003) Coronavirus main proteinase (3CLpro) structure: Basis for design of anti-SARS drugs, *Science 300*, 1763−7.
12. Lee, T.-W., Cherney, M. M., Huitema, C., Liu, J., James, K. E., Powers, J. C., Eltis, L. D., and James, M. N. G. (2005) Crystal structures of the main peptidase from the SARS coronavirus inhibited by a substrate-like aza-peptide epoxide, *J. Mol. Biol. 353*, 1137−51.
13. Shi, J. H., Wei, Z., and Song, J. X. (2004) Dissection study on the SARS 3C-like protease reveals the critical role of the extra domain in dimerization of the enzyme: Defining the extra domain as a new target for design of highly-specific protease inhibitors, *J. Biol. Chem. 279*, 24765−73.
14. Huang, C., Wei, P., Fan, K., Liu, Y., and Lai, L. (2004) 3C-like proteinase from SARS coronavirus catalyzes substrate hydrolysis by a general base mechanism, *Biochemistry 43*, 4568−74.
15. Yang, H., Yang, M., Ding, Y., Liu, Y., Lou, Z., Zhou, Z., Sun, L., Mo, L., Ye, S., Pang, H., Gao, G. F., Anand, K., Bartlam, M., Hilgenfeld, R., and Rao, Z. (2003) The Crystal Structure of Severe Acute Respiratory Syndrome Virus Main Protease and its Complex with an Inhibitor, *Proc. Natl. Acad. Sci. U.S.A. 100*, 13190−5.
16. Chen, H., Wei, P., Huang, C., Tan, L., Liu, Y., and Lai, L. (2006) Only one protomer is active in the dimer of SARS 3C-like proteinase, *J. Biol. Chem. 281*, 13894−8.
17. Fan, K., Wei, P., Feng, Q., Chen, S., Huang, C., Ma, L., Lai, B., Pei, J., Liu, Y., Chen, J., and Lai, L. (2004) Biosynthesis, purification and substrate specificity of servere acute respiratory syndrome coronavius 3C-like proteinase, *J. Biol. Chem. 279*, 1637−42.
18. Chou, C.-Y., Chang, H.-C., Hsu, W.-C., Lin, T.-Z., Lin, C.-H., and Chang, G.-G. (2004) Quaternary structure of the severe acute respiratory syndrome (SARS) coronavirus main protease, *Biochemistry 43*, 14958−70.
19. Kuo, C. J., Chi, Y. H., Hsu, J. T., and Liang, P. H. (2004) Characterization of SARS main protease and inhibitor assay using a fluorogenic substrate, *Biochem. Biophys. Res. Commun. 318*, 862−7.
20. Chen, S., Chen, L., Tan, J., Chen, J., Du, L., Sun, T., Shen, J., Chen, K., Jiang, H., and Shen, X. (2005) Severe acute respiratory syndrome coronavirus 3C-like proteinase N terminus is indispensable for proteolytic activity but not for enzyme dimerization, *J. Biol. Chem. 280*, 164−73.
21. Hsu, W.-C., Chang, H. C., Chou, C.-Y., Tsai, F.-J., Lin, P.-I., and Chang, G.-G. (2005) Critical assessment of important regions in the subunit association and catalytic action of the severe acute respiratory syndrome coronavirus main protease, *J. Biol. Chem. 280*, 22741−8.
22. Hsu, M. F., Kuo, C. J., Chang, K. T., Chang, H. C., Chou, C. C., Ko, T. P., Shr, H. L., Chang, G. G., Wang, A. H.-J., and Liang, P.-H. (2005) Mechanism of the maturation process of SARS-CoV 3CL protease, *J. Biol. Chem. 280*, 31257−66.
23. Wei, P., Fan, K., Chen, H., Ma, L., Huang, C., Tan, L., Xi, D., Li, C., Liu, Y., Cao, A., and Lai, L. (2006) The N-terminal octapeptide acts as a dimerization inhibitor of SARS coronavirus 3C-like proteinase, *Biochem. Biophys. Res. Commun. 339*, 865−72.
24. Graziano, V., McGrath, W. J., DeGruccio, A. M., Dunn, J. J., and Mangel, W. F. (2006) Enzymatic activity of the SARS coronavirus main proteinase dimer, *FEBS Lett. 580*, 2577−83.
25. Mangel, W. F., Toledo, D. L., Brown, M. T., Martin, J. H., and McGrath, W. J. (1996) Characterization of three components of human adenovirus proteinase activity *in vitro*, *J. Biol. Chem. 271*, 536−43.
26. Bewley, M. C., Graziano, V., Jiang, J., Matz, E., Studier, F. W., Pegg, A. E., Coleman, C. S., and Flanagan, J. M. (2006) Structures of wild-type and mutant human spermidine/spermine N1-acetyltransferase, a potential therapeutic drug target, *Proc. Natl. Acad. Sci. U.S.A. 103*, 2063−8.
27. Svergun, D., Barberato, C., and Koch, M. H. J. (1995) CRYSOL: A Program to Evaluate X-ray Solution Scattering of Biological Macromolecules from Atomic Coordinates, *J. Appl. Crystallogr. 28*, 768−73.
28. Konarev, P. V., Volkov, V. V., Sokolova, A. V., Koch, M. H. J., and Svergun, D. I. (2003) PRIMUS: A Windows PC-based system for small-angle scattering data analysis, *J. Appl. Crystallogr. 36*, 1277−82.
29. Guinier, A., and Fournet, B. (1955) *Small Angle Scattering of X-rays*, Wiley, New York.
30. Glatter, O. (1982) *Small Angle X-ray Scattering*, Academic Press, San Diego.
31. Hubbard, S. R., Hodgson, K. O., and Doniach, S. (1988) Small-angle X-ray scattering investigation of the solution structure of troponin C, *J. Biol. Chem. 263*, 4151−8.
32. Silva, J. L., Oliveria, A. C., Gomes, A. M., Lima, L. M., Mohana-Borges, R., Pacheco, A. B., and Foguel, D. (2002) Pressure induces folding intermediates that are crucial for protein-DNA recognition and virus assembly, *Biochim. Biophys. Acta 1595*, 250−65.
33. Grant, S. K., Deckman, I. C., Culp, J. S., Minnich, M. D., Brooks, I. S., Hensley, P., Debouck, C., and Meek, T. D. (1922) Use of protein unfolding studies to determine the conformational and dimeric stabilities of HIV-1 and SIV proteases, *Biochemistry 31*, 9491−501.
34. Xie, D., Gulnik, S., Gustchina, E., Yu, B., Shao, W., Qoronfleh, W., Nathan, A., and Erickson, J. W. (1999) Drug resistance mutations can effect dimer stability of HIV-1 protease at neutral pH, *Protein Sci. 8*, 1702−7.
35. Jordan, S. P., Zugay, J., Darke, P. L., and Kuo, L. C. (1992) Activity and dimerization of human immunodeficiency virus protease as a function of solvent composition and enzyme concentration, *J. Biol. Chem. 267*, 20028−32.
36. Kuzmic, P. (1993) Kinetic assay for HIV protease subunit dissociation, *Biochem. Biophys. Res. Commun. 191*, 998−1003.
37. Margosiak, S. A., Vanderpool, D. L., Sisson, W., Pinko, C., and Kan, C.-C. (1996) Dimerization of the human cytomegalovirus protease: Kinetic and biochemical characterization of the catalytic homodimer, *Biochemistry 35*, 5300−7.
38. Pray, T. R., Kinkead-Reiling, K., Demirjian, B. G., and Craik, C. S. (2002) Conformational change coupling the dimerization and activation of KSHV protease, *Biochemistry 41*, 1474−82.
39. Peters, H., Kusov, Y. Y., Meyer, S., Benie, A. J., Bauml, E., Wolff, M., Rademacher, C., Peters, T., and Gauss-Muller, V. (2005) Hepatitis A virus proteinase 3C binding to viral RNA: Correlation with substrate binding and enzyme dimerization, *Biochem. J. 385*, 363−70.
40. Wlodawer, A., Miller, M., Jaskolski, M., Sathyanarayana, B. K., Baldwin, E., Weber, I. T., Selk, L. M., Clawson, L., Schneider, J., and Kent, S. B. (1989) Conserved folding in retroviral proteases: Crystal structure of a synthetic HIV-1 protease, *Science 245*, 616−21.
41. Navia, M. A., Fitzgerald, P. M., McKeever, B. M., Leu, C. T., Heimbach, J. C., Herber, W. K., Sigal, I. S., Darke, P. L., and Springer, J. P. (1989) Three-dimensional structure of aspartyl protease from human immunodeficiency virus HIV-1, *Nature 337*, 615−20.
42. Burstein, H., Bizub, D., and Skalka, A. M. (1991) Assembly and processing of avian retroviral Gag polyproteins containing linked protease dimers, *J. Virol. 65*, 6165−72.
43. Krausslich, H. G. (1991) Human immunodeficiency virus proteinase dimer as component of the viral polyprotein prevents particle assembly and viral infectivity, *Proc. Natl. Acad. Sci. U.S.A. 88*, 3213−7.

BI061746Y